Design and Trajectory Optimization of a Shape-Morphing Aeroshell for Skip-Entry Orbital Inclination Change

Abinay Brown* and Glen Chou†
Georgia Institute of Technology, Atlanta, Georgia, 30318

This paper addresses the gap between the theoretical efficiency of skip-entry maneuvers for orbital inclination change and the practical difficulty of achieving the high lift-to-drag (L/D) ratios required with conventional rigid aeroshells. We propose a modular, shape-morphing aeroshell that attaches to an existing spacecraft and uses actuated arms to vary its geometry, enabling active control of aerodynamic coefficients during hypersonic skip. We model the shape-morphing aerodynamics, equations of motion, Δi and ΔV relationships for skip-entry, and formulate an optimal control problem to determine arm deflections, angles of attack, and bank angles that minimize total ΔV while achieving a desired inclination change Δi. Our results show practical ΔV reductions of 24–38% for $\Delta i = 0°$ to $18°$, and approximately 40% for large changes of $28.5°$ and $47.1°$, corresponding to transfers from $i = 70°$ and $i = 51.6°$ to sun-synchronous orbit ($i = 98.5°$), compared to pure propulsive plane change.

I. Nomenclature

$\vec{V}$	=	Freestream Velocity vector, m/s
η	=	Local flow-surface inclination angle between $\vec{V}$ and $\hat{n}$, rad
C_p	=	Local pressure coefficient
$C_{p,\max}$	=	Newtonian pressure coefficient for hypersonic flow
A	=	Area, m^2
$\hat{i}, \hat{j}, \hat{k}$	=	XYZ unit vectors
C_A, C_N, C_T	=	Axial, Normal, Tangential Aerodynamic force coefficients
C_L, C_D, C_Y	=	Lift, Drag, Side-Force coefficients
L, D, Y	=	Lift, Drag, Side-Force
S	=	Total Reference Area, m^2
r	=	Radial distance from Earth center, m
ϕ	=	Geocentric latitude, rad
θ	=	Geocentric longitude, rad
V_R	=	Reentry velocity in LVLH frame, m/s
γ	=	Flight-path angle, rad
ψ	=	Heading/Azimuth angle, rad
α	=	Angle of Attack, rad
β	=	Sideslip angle, rad
σ	=	Bank angle, rad
h	=	Altitude, m
ρ	=	Atmospheric density, kg/m^3
H	=	Atmospheric scale height, m
g	=	Gravitational acceleration, m/s^2
μ	=	Earth gravitational parameter, m^3/s^2
$\omega_\oplus$	=	Earth angular velocity, rad/s
m	=	Vehicle mass, kg
r_n	=	Aeroshell nose radius, m
l	=	Aeroshell arm length, m

*Graduate Student, Daniel Guggenheim School of Aerospace Engineering, 756 W Peachtree St NW, Atlanta, GA 30308.
†Assistant Professor, Schools of Cybersecurity & Privacy and Aerospace Engineering, 756 W Peachtree St NW, Atlanta, GA 30308.

h	=	Specific angular momentum, m^2/s
$\dot{q}$	=	Convective heat rate, W/m^2
$\vec{r}$	=	Position vector, m
$\vec{v}$	=	Velocity vector, m/s
u	=	Aeroshell arm control angle, deg
i	=	Orbital inclination (rad)
t	=	Time (s)
GMST	=	Greenwich Mean Sidereal Time (rad)

Subscripts

j	=	jth control arm or aeroshell face
0	=	Initial
SL	=	Sea-Level
f	=	final
$\oplus$	=	Earth

Superscripts

ECF	=	Earth-Centered-Fixed coordinate frame
ECI	=	Earth-Centered-Inertial coordinate frame
ENU	=	Topocentric coordinate frame

II. Introduction and Motivation

Skipping-entry is an atmospheric reentry technique, where a vehicle briefly "skips" along the upper atmosphere to reduce speed, lower peak heating, and increase cross-range distance for maneuverability. Beyond traditional reentry, skip-entry can also serve as an aeroassist method for orbital inclination change, allowing a spacecraft to use the atmospheric medium to shift into a different orbital plane more efficiently compared to pure plane-change maneuvers. A pure plane change maneuver requires the spacecraft to perform a tangential orbital burn to change its inclination, which requires high ΔV and significant fuel mass. As such, an efficient plane change maneuver could be beneficial to save fuel for orbital reconnaissance missions, scientific orbital missions, or even for on-orbit-servicing (OOS) that may required reaching multiple orbital inclinations.

A prior parametric design analysis [1][2] has shown that skip-entry maneuver requires 50–85% less ΔV, enabling a maximum inclination change of 19.91° in a single skip, compared to a purely propulsive plane-change maneuver, which is fuel-inefficient and not practically implementable. In particular, these studies optimized for an ideal trans-atmospheric-vehicle (TAV) design, identifying optimal skip-entry boundary conditions and idealized aerodynamic and mass parameters. Although this highlights the theoretical efficiency of skip-entry, it does not address the practical design challenges required for a real vehicle to achieve such performance, especially for an in-orbit spacecraft/satellite. A key limitation is the assumed aerodynamic requirement: [1] found that a lift/drag (L/D) ratio of 6 is needed to achieve the reported ΔV savings, corresponding to a lift coefficient $C_L = 3$ and drag coefficient $C_D = 0.5$. For context, even the Space Shuttle, a TAV/space-plane that was designed to be aerodynamic, at best only achieved an L/D ratio of only about 1.9 at an angle of attack of 17.9° in the hypersonic regime [3]. Additionally, there are no existing aeroshell approaches that enable the aerodynamic performance needed to execute an efficient skip-entry maneuver, revealing a major gap between theoretical predictions and practical feasibility for in-orbit spacecraft/satellites.

Deployable heat shields/aeroshell concepts have been previously studied for atmospheric reentry cases and have been previously flight tested. The Hypersonic Inflatable Aerodynamic Decelerator (HIAD) [4], in particular, is an inflatable, flexible structure that forms a large aeroshell around a spacecraft [5], increasing drag area and reducing the ballistic coefficient to lower peak deceleration loads and thermal heating during reentry. HIAD was demonstrated successfully in the LOFTID experiment [6]. ADEPT (Adaptable Deployable Entry and Placement Technology) is another low-ballistic-coefficient concept using umbrella-like ribs and struts to deploy a flexible carbon-fabric skin as a heat shield, which was successfully tested on a sounding rocket [7]. Shape-morphing aeroshells have also been previously studied as a form of guidance, specifically for atmospheric reentry [8]. However, while skip-entry for orbital inclination change has been theoretically studied before with fixed, static aerodynamic parameters, it has not been practically implemented.

To address these limitations, we propose a modular *shape-morphing* aeroshell heat shield that attaches to an existing spacecraft and enables practical skip-entry orbital plane-change maneuvers. The concept is based on a variable-geometry aeroshell capable of adjusting its outer shape during atmospheric skip. Active control of the geometry control the aerodynamic forces of the spacecraft to perform the skip maneuver. This avoids the need for a high-L/D lifting-body vehicle while still enabling the aerodynamic performance required for the maneuver. In particular, by developing the novel enabling technology of a modular, shape-morphing aeroshell, our approach bridges the gap between the theoretical efficiency of skip-entry for orbital plane change and the aerodynamic impracticality of achieving the required L/D with rigid axis-symmetric blunted aeroshells. The proposed shield provides temporary aerodynamic authority during atmospheric skip, allowing a spacecraft to perform a skip-entry maneuver to alter its inclination without expending significant propellant. Its modular design enables integration onto a broad range of spacecraft without requiring a full vehicle redesign into a TAV that requires high structural mass and solving heating challenges.

A. Contributions

In this paper, we identify the major barriers in current skip-entry research and present the motivation behind the morphing aeroshell solution. We outline the key design requirements, including optimal trajectory design, thermal limits, aero loads, and mass. Our contributions in this abstract are as follows:

- We introduce a modular, variable-geometry aeroshell that attaches to existing spacecraft. By actively adjusting its outer shape during atmospheric skip, the aeroshell increases effective lift, redistributes heating, and reduces drag, enabling skip-entry orbital plane-change maneuvers without requiring a high-L/D rigid TAV.
- We perform detailed aerodynamic and thermal analyses to evaluate the feasibility of the shape-morphing aeroshell. In particular, we calculate peak heating rates and integrated heat loads to ensure the thermal protection system (TPS) can withstand aerothermal stresses. Our detailed aerodynamic analysis is also used to derive the dynamics used in downstream trajectory planning to achieve the desired inclination plane change.
- We formulate and solve a nonlinear optimal control problem, where we find the optimal trajectory $(r, \theta, \phi, V, \gamma, \psi)$ and control inputs (arm angles, angle of attack, and bank angle) that minimizes the deorbit and re-circularization ΔV for varying inclination changes Δi.
- We evaluate our proposed shape-morphing aeroshell in simulation, demonstrating that it can perform skip-entry maneuvers to achieve orbital inclination changes up to 47°, reducing the required ΔV by up to 40% compared to purely propulsive plane-change maneuvers. These large inclination changes are feasible with manageable thermal and structural loads, though they require higher aerodynamic forces and thicker thermal protection, highlighting a trade-off between efficiency and vehicle design constraints.

III. Methodology

We provide an overview of our method. First, we derive analytical expressions for the aerodynamic coefficients of the shape morphing aeroshell, using Newtonian hypersonic flow theory, as a function of the arm control angles which control the geometry of the aeroshell (Section III.A). Then, we leverage the derived coefficients to introduce the equations of motion that govern the skip trajectories (Section III.B). Next, we present the coordinate frame conversion to estimate the inclination change and the instantaneous ΔV required for de-orbit and re-circularization during the skip maneuver (Section III.C). We leverage these derivations to formulate an optimal control problem that solves for the optimal aeroshell shapes and angle of attack and bank angles needed to achieve a given inclination change while minimizing the required total ΔV for the skip entry maneuver (Section III.D). Finally, we also perform an aerothermal analysis (Section III.E) to quantify the thermal loads that the spacecraft is subjected to during the maneuver.

A. Aeroshell Modeling

In this section, we will overview the design of our aeroshell (Section III.A.1) and leverage Newtonian hypersonic flow theory (Section III.A.2) to determine its aerodynamic coefficients.

1. Aeroshell Design

We model the proposed aeroshell as an octagonal structure inspired by the ADEPT concept [9], but with a key distinction: each deployable arm can independently control its deflection angle, enabling active shape morphing for aerodynamic authority during skip-entry. The eight arms support eight flat triangular panels (Figures 1 and **??**), and each arm is permitted to vary its deployment angle between 18° and 70° relative to the axial direction. This actuation range allows the aeroshell to transition among multiple geometric configurations to adjust lift, drag, and heating throughout the maneuver. Although not shown in the figure, a blunt hemispherical nose cone of constant radius is included to maintain acceptable thermal loads during atmospheric skip. While additional arms could provide smoother curvature and finer control, they also increase structural mass and engineering complexity. For the case study in Section III.F, we found that eight arms strike a practical balance between aerodynamic performance and mass efficiency.

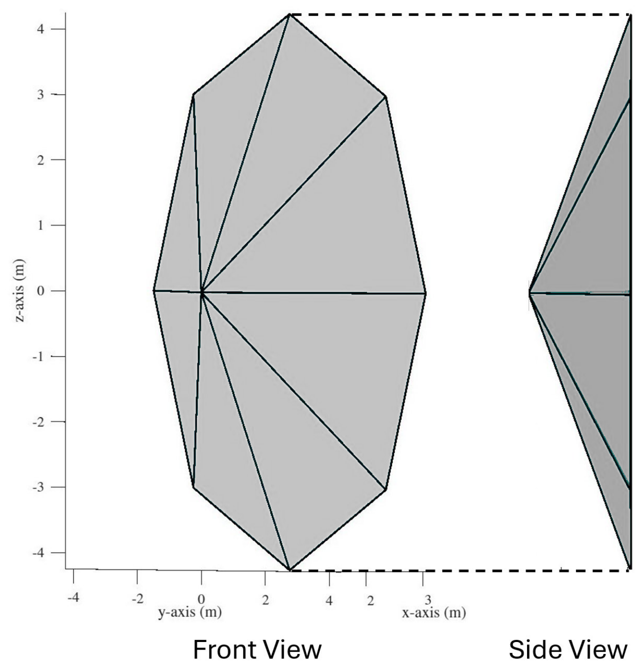

Fig. 1 Idealized octagonal flat-plate shape-morphing aeroshell design.

The aeroshell skin is assumed to be a flexible, elastic carbon–carbon fabric, similar to ADEPT's construction. This material choice allows the arms to fold completely flush with the spacecraft when stowed, preserving modularity, while providing a taut surface with no slack when deployed. This results overall in a smooth, aerodynamically efficient profile.

2. Newtonian Theory for Hypersonic Flow

We made use of Newtonian hypersonic flow theory [10] to analytically determine the aerodynamic coefficients (C_L, C_D, C_Y) of the morphing aeroshell as functions of the individual arm deflection angles that shape the aeroshell geometry (Fig. 1). Under this model, fluid particles are assumed to travel in straight-line trajectories until they impact the surface, where all normal momentum is lost and only tangential momentum is conserved. As a result, the surface pressure depends solely on the loss of normal momentum, leading to closed-form expressions for the pressure coefficient. For each flat plate, the free-stream velocity V_∞ is transformed into the local velocity vector using the angle of attack and sideslip, as expressed in (1).

$$\vec{V}_\infty = V_\infty \cos\alpha \cos\beta \hat{i} + V_\infty \sin\beta \hat{j} + V_\infty \sin\alpha \cos\beta \hat{k} \tag{1}$$

The corresponding angle of incidence η is computed, where $\hat{n}$ denotes the unit surface normal of the plate and the pressure coefficient is then obtained from (2), assuming a Newtonian stagnation-point maximum pressure coefficient of $C_{p,\max} = 2$.

$$\cos\eta = \frac{\vec{V} \cdot \hat{n}}{\|\vec{V}\|\|\hat{n}\|}, \qquad C_p = C_{p,\max} \cos^2\eta \tag{2}$$

Crucially, this formulation enables analytical evaluation of the aeroshell's aerodynamic response for any control-induced shape configuration, which will be critical for downstream trajectory optimization in Section III.D. The axial, normal, and tangential force coefficients are obtained by integrating the pressure coefficient over the surface in their respective directions. Since the aeroshell is modeled as set of eight isosceles flat plates, the coefficients are computed individually for each triangular flat plates using (3), (4), and (5) [10] in 3D.

$$C_{A,j} = \frac{1}{A_j^{\text{ref}}} \iint C_p (\hat{V}_\infty \cdot \hat{n})^2 \hat{n}_x \, dA, \quad \forall j \in \{1, \ldots, 8\} \tag{3}$$

$$C_{N,j} = \frac{1}{A_j^{\text{ref}}} \iint C_p (\hat{V}_\infty \cdot \hat{n})^2 \hat{n}_z \, dA, \quad \forall j \in \{1, \ldots, 8\} \tag{4}$$

$$C_{T,j} = \frac{1}{A_j^{\text{ref}}} \iint C_p (\hat{V}_\infty \cdot \hat{n})^2 \hat{n}_y \, dA \quad \forall j \in \{1, \ldots, 8\} \tag{5}$$

Where $\hat{V}_\infty$ is the normalized free-stream velocity vector in (1)), C_p is as defined in (2), $(\hat{n}_x, \hat{n}_y, \hat{n}_z)$ are the (x, y, z) components of the surface normal vector $\hat{n}$, A_j^{ref} is the frontal surface area for plate j, and the double integral is evaluated over the wetted surface area for plate j. The wetted surface area of each panel is determined from the cross product of its defining arm vectors, while the projected reference area is computed via the dot product with the $\hat{i}$ unit vector (along the x-axis in Figure 1). This approach yields full 3D aerodynamic coefficients that vary directly with the arm-controlled geometry. Then, the total axial, normal, and tangential (C_A, C_N, C_T) contributions of all eight plates are found using the sum of the individual coefficients normalized by their area ratios.

$$C_A = \sum_{j=1}^{8} \frac{A_{\text{ref}}^j}{S} C_{A,j}, \quad C_N = \sum_{j=1}^{8} \frac{A_{\text{ref}}^j}{S} C_{N,j}, \quad C_T = \sum_{j=1}^{8} \frac{A_{\text{ref}}^j}{S} C_{T,j} \tag{6}$$

Where $S = \sum_{j=1}^{8} A_{\text{ref}}^j$ is the total frontal area. Additionally, we include a constant-radius blunt nose that contributes to drag but is necessary to maintain manageable heating rates under the Sutton–Graves model [11]. Without this blunt forebody, a sharp nose would produce theoretically unbounded stagnation heating, making the vehicle thermally infeasible. Finally, the axial, tangential, and normal force coefficients are transformed to drag, side force, and lift coefficients (C_D, C_Y, C_L) given by the transformation in (7), where we assume that the angle of sideslip is zero.

$$\begin{bmatrix} C_D \\ C_Y \\ C_L \end{bmatrix} = \begin{bmatrix} \cos\alpha\cos\beta & \sin\beta & \sin\alpha\cos\beta \\ \cos\alpha\sin\beta & \cos\beta & -\sin\alpha\sin\beta \\ -\sin\alpha & 0 & \cos\alpha \end{bmatrix} \begin{bmatrix} C_A \\ C_T \\ C_N \end{bmatrix} \tag{7}$$

B. Skip-Entry Equations of Motion

We adopt the nonplanar reentry equations of motion presented in [12] and modify them for our shape-morphing aeroshell in (8)–(13). The vehicle is assumed to be unpowered throughout the skip maneuver, with thrust applied only as impulsive burns at the boundaries for de-orbit and re-circularization. Because these burns occur outside the atmospheric skip, they do not affect the inclination change generated by aerodynamic forces; modeling them as instantaneous simplifies the formulation while preserving the skip dynamics of interest. Furthermore, due to the asymmetric geometries induced by the morphing aeroshell, we re-derived the equations from [12] to incorporate lateral (side) aerodynamic forces. These equations are expressed in the Local-Vertical-Local-Horizontal (LVLH) frame. For brevity, $s_{(\cdot)}$, $c_{(\cdot)}$, and $t_{(\cdot)}$ refer to $\sin(\cdot)$, $\cos(\cdot)$, and $\tan(\cdot)$, respectively.

$$\dot{r} = V_R s_\gamma \tag{8}$$

$$\dot{\theta} = \frac{V_R c_\gamma c_\psi}{r c_\phi} \tag{9}$$

$$\dot{\phi} = \frac{V_R c_\gamma s_\psi}{r} \tag{10}$$

$$\dot{V}_R = -\frac{D}{m} - g(r) s_\gamma + r\omega_\oplus^2 c_\phi (c_\phi s_\gamma - s_\phi s_\psi c_\gamma) \tag{11}$$

$$\dot{\gamma} = \frac{1}{V_R}\Big[\frac{L}{m}c_\sigma + \frac{Y}{m}\sin\sigma - g(r)c_\gamma + \frac{V_R^2}{r}c_\gamma + 2V_R\omega_\oplus c_\phi c_\psi + r\omega_\oplus^2 c_\phi(c_\phi c_\gamma + s_\phi s_\psi s_\gamma)\tag{12}$$

$$\dot{\psi} = \frac{1}{V_R}\Big[\frac{L}{m}\frac{s_\sigma}{c_\gamma} - \frac{Y}{m}\frac{c_\sigma}{c_\gamma} - \frac{V_R^2}{r}c_\gamma c_\psi t_\phi + 2V_R\omega_\oplus(s_\psi c_\phi t_\gamma - s_\phi) - \frac{r\omega_\oplus^2 s_\phi c_\phi c_\psi}{c_\gamma}\Big]\tag{13}$$

In particular, the gravitational acceleration $g(r)$ is a function of radial distance, as given by (14). We adopt an exponential atmospheric model (15) rather than Earth-GRAM [13] or other tabulated models, since a continuously differentiable function is required for the trajectory optimizer to perform automatic differentiation.

$$g(r) = g_{\mathrm{SL}}\left(\frac{r_\oplus}{r}\right)^2\tag{14}$$

$$\rho(h) = \rho_{SL}\,\exp\left(-\frac{h}{H}\right), \quad \text{with } h = r - r_\oplus\tag{15}$$

Finally, the lift, drag, and side-force (L, D, Y) expressions are given by (16), where the total reference area S and the aerodynamic coefficients C_L, C_D, and C_Y depend on the aeroshell geometry (i.e., the control angles) and the angle of attack.

$$L = \frac{1}{2}\rho C_L(\alpha,u)S(\alpha,u)V_R^2, \quad D = \frac{1}{2}\rho C_D(\alpha,u)S(\alpha,u)V_R^2, \quad Y = \frac{1}{2}\rho C_Y(\alpha,u)S(\alpha,u)V_R^2\tag{16}$$

C. Inclination Change and Required ΔV

To determine the inclination change Δi produced by the skip-entry maneuver, we convert the boundary conditions from the LVLH frame to the Earth-Centered-Inertial (ECI) frame following [14]. The orbital inclination is then computed at the entry and exit of the skip, and their difference defines Δi. To perform this conversion, the LVLH states are first transformed into the Earth-Centered Fixed (ECF) frame to obtain the vehicle position, using (17)

$$\vec{r}^{\,\mathrm{ECF}} = \begin{bmatrix} r\cos\phi\cos\theta & r\cos\phi\sin\theta & r\sin\phi \end{bmatrix}^T\tag{17}$$

To then convert the velocity from the LVLH frame to the ECF frame, we first map the state to the topocentric frame using (18). Subsequently, we convert the state from the topocentric frame to the ECF frame using (19).

$$\vec{v}^{\,\mathrm{ENU}} = \begin{bmatrix} v\cos\gamma\cos\psi & v\cos\gamma\sin\psi & v\sin\gamma \end{bmatrix}^T\tag{18}$$

$$\vec{v}^{\,\mathrm{ECF}} = \begin{bmatrix} -\sin\theta & -\sin\phi\cos\theta & \cos\phi\cos\theta \\ \cos\theta & -\sin\phi\sin\theta & \cos\phi\sin\theta \\ 0 & \cos\phi & \sin\phi \end{bmatrix}\vec{v}^{\,\mathrm{ENU}}\tag{19}$$

To convert from the ECF frame to the ECI frame, we assume a Greenwich Mean Sidereal Time (GMST) of zero ($\Theta_{\mathrm{GMST}} = 0$). Since the skip-entry maneuver lasts only a few minutes, we simplify the transformation by applying a rotation about the z-axis based solely on the Earth's angular velocity; the rotation after the maneuver is given by $\Theta_f = \Theta_{\mathrm{GMST}} + \omega_\oplus T_{\mathrm{elapsed}}$. To obtain the ECI state at the terminal time instant T_{elapsed}. The corresponding rotation matrix $R_z(\Theta)$ is provided in (20). For the initial state, the elapsed time is zero, so, ($\Theta_0 = 0$), so the rotation reduces to the identity matrix.

$$R_z(\Theta) = \begin{bmatrix} \cos\Theta & -\sin\Theta & 0 \\ \sin\Theta & \cos\Theta & 0 \\ 0 & 0 & 1 \end{bmatrix}\tag{20}$$

Using (21), we find the inertial positions at the initial and final state. Similarly, we use (22) to find the ECF velocity at the boundary conditions.

$$\vec{r}_0^{\,\mathrm{ECI}} = R(\Theta_0)\vec{r}_0^{\,\mathrm{ECF}}, \qquad \vec{r}_f^{\,\mathrm{ECI}} = R(\Theta_f)\vec{r}_f^{\,\mathrm{ECF}}\tag{21}$$

$$\vec{v}_0^{\,\mathrm{ECI}} = R(\Theta_0)(\vec{v}_0^{\,\mathrm{ECF}} + \vec{\omega}_\oplus \times \vec{r}_0^{\,\mathrm{ECF}}), \qquad \vec{v}_f^{\,\mathrm{ECI}} = R(\Theta_f)(\vec{v}_f^{\,\mathrm{ECF}} + \vec{\omega}_\oplus \times \vec{r}_f^{\,\mathrm{ECF}})\tag{22}$$

For the inclination change, we first find the specific angular momentum vector given by (23). The orbital inclination at the boundary conditions is then determined from (24), and the difference between the initial inclination i_0 and the final inclination i_f gives the inclination change Δi.

$$\vec{h}_0 = \vec{r}_0^{\mathrm{ECI}} \times \vec{v}_0^{\mathrm{ECI}}, \quad \vec{h}_f = \vec{r}_f^{\mathrm{ECI}} \times \vec{v}_f^{\mathrm{ECI}} \tag{23}$$

$$i_0 = \arccos \frac{h_0 \cdot \hat{k}}{\|\vec{h}_0\|}, \quad i_f = \arccos \frac{h_f \cdot \hat{k}}{\|\vec{h}_f\|}, \quad \Delta i = |i_f - i_0| \tag{24}$$

For the ΔV required for de-orbit and re-circularization, we first compute the equivalent circular orbit velocity vector in the ECI frame at the boundary conditions. This involves computing the circular orbit velocity unit vector using (25), followed by determining the required circular orbital speed of the initial and final orbit using (26).

$$\hat{v}_{0,\mathrm{circ}}^{\mathrm{ECI}} = \frac{\vec{h}_0 \times \vec{r}_0}{\|\vec{h}_0 \times \vec{r}_0\|}, \quad \hat{v}_{f,\mathrm{circ}}^{\mathrm{ECI}} = \frac{\vec{h}_f \times \vec{r}_f}{\|\vec{h}_f \times \vec{r}_f\|} \tag{25}$$

$$V_{0,\mathrm{circ}} = \sqrt{\frac{\mu}{\|\vec{r}_0^{\mathrm{ECI}}\|}}, \quad V_{f,\mathrm{circ}} = \sqrt{\frac{\mu}{\|\vec{r}_f^{\mathrm{ECI}}\|}} \tag{26}$$

Finally, using (27), we compute the ΔV required for de-orbit and re-circularization associated with performing a skip trajectory for orbital inclination change. In this analysis, we assume that the ΔV is applied instantaneously.

$$\Delta V_{\mathrm{deorbit}} = \|\vec{v}_0^{\mathrm{ECI}} - V_{0,\mathrm{circ}}\hat{v}_{0,\mathrm{circ}}^{\mathrm{ECI}}\|, \quad \Delta V_{\mathrm{recirc}} = \|\vec{v}_f^{\mathrm{ECI}} - V_{f,\mathrm{circ}}\hat{v}_{f,\mathrm{circ}}^{\mathrm{ECI}}\| \tag{27}$$

D. Optimal Control Problem Formulation

Using the dynamics $\dot{\mathbf{x}} = f(\mathbf{x}(t), \mathbf{u}(\mathbf{t}))$ derived in (8)–(13), where $\mathbf{x} = [r, \theta, \phi, V_R, \gamma, \psi]^\top$ and $\mathbf{u} = [u_1, \ldots, u_8, \alpha, \sigma]^\top$, and incorporating the analytical expressions for the aerodynamic coefficients as functions of the arm control angles $u_1, \ldots, u_8$ that shape-morph the aeroshell, we solve an optimal control problem using direct transcription with multiple shooting. This determines the optimal sequence of aeroshell shapes, angle of attack, and bank angles required to achieve a target inclination change while minimizing the total ΔV for de-orbit and re-circularization, as defined in Section III.C and formalized in problem (28).

$$\begin{aligned}
\min_{\mathbf{x}(t),\mathbf{u}(t)} \quad & J := \|\vec{v}_0^{\mathrm{ECI}} - V_{0,\mathrm{circ}}\hat{v}_{0,\mathrm{circ}}^{\mathrm{ECI}}\|^2 + \|\vec{v}_f^{\mathrm{ECI}} - V_{f,\mathrm{circ}}\hat{v}_{f,\mathrm{circ}}^{\mathrm{ECI}}\|^2 \\
\text{subject to} \quad & \dot{\mathbf{x}}(t) = f(\mathbf{x}(t), \mathbf{u}(t)), \quad \forall t \in [t_0, t_f] \\
& r(t_0) \geq 130\mathrm{km} + r_\oplus, \quad \phi(t_0) = 0, \quad \theta(t_0) = 0, \quad \psi(t_0) = 0, \quad -\frac{\pi}{2} \leq \gamma(t_0) \leq 0 \\
& r(t_f) \geq 130\mathrm{km} + r_\oplus, \quad 0 \leq \psi(t_f) \leq 25^\circ, \quad 0 \leq \gamma(t_f) \leq \frac{\pi}{2} \\
& 18^\circ \leq u_j(t) \leq 70^\circ, \quad \forall j = 1, \ldots, 8, \quad \forall t \in [t_0, t_f] \\
& -10^\circ \leq \alpha(t) \leq 10^\circ, \quad \forall t \in [t_0, t_f] \\
& -90^\circ \leq \beta(t) \leq 90^\circ, \quad \forall t \in [t_0, t_f]
\end{aligned} \tag{28}$$

For practical implementation, the trajectory is time-discretized with 50 time steps, where the final time is treated as a free optimization variable. Allowing a free final time prevents the optimization from being overly constrained, which could otherwise lead to suboptimal skip trajectories that do not minimize the required ΔV. Here, the control arms are restricted to a maximum of 70°, which is the limit for most axis-symmetric aeroshells, with a minimum limit of 18° to accommodate a spacecraft of size 1.5m ×1.5m ×1.5m. We also limit the angle of attack α to a maximum of ±10°, both because the maximum lift-to-drag ratio occurs within this range and, more importantly, to provide sufficient shielding of the spacecraft's aft section from hypersonic flow. Additionally, the initial flight path angle is constrained to be below the horizon at de-orbit (entry), and the final flight path angle is constrained to be above the horizon at re-circularization (exit). The resulting nonlinear program is transcribed in CasADi [15] and solved using the IPOPT optimizer [16]. Initial attempts to directly impose the target inclination change Δi as a nonlinear constraint led to poor convergence and frequent infeasibility. Instead, we perform a sequence of optimizations in which the terminal heading angle is indirectly constrained over a range of 0° to 25°. After convergence, the corresponding inclination change Δi is computed using the relations in Section III.C.

E. Aerothermal Heating

To estimate aerothermal heating, we apply the Sutton–Graves correlation [11] for stagnation-point convective heating and interpolate the Tauber–Sutton model [17] to assess stagnation-point radiative heating. For the skip-entry flight regime considered, convective heating dominates, and radiative heating is negligible. Consequently, we report aerothermal loads based solely on the convective heating component.

$$\dot{q} = 1.83 \times 10^{-4} \sqrt{\frac{\rho}{r_n}} V^3 \quad [\mathrm{W/m^2}] \tag{29}$$

F. Case Study: Inclination Sweep & Large Inclination Maneuvers

In our simulation case study, we assume the spacecraft begins the skip maneuver at the equator with an initial inclination $i_0 = 0$ ($\psi_0 = 0°$, $\theta_0 = 0°$, $\phi_0 = 0°$). The vehicle transitions to a higher-inclination orbit, represented by a positive terminal heading angle. This inclination change is independent of the specific initial and final latitude and longitude values used in the study.

1. Δi vs. ΔV for $\Delta i = 1°, \ldots, 25°$

For our initial case study, we sweep the inclination change Δi from 1° to 20° and determine the required ΔV by solving the optimal control problem (28) with the previously described constraints, following an approach similar to [1]. This enables us to characterize the performance trends and quantify fuel savings of the skip-entry maneuver in comparison with a purely propulsive plane-change maneuver.

2. Large Inclination Change $\Delta i = 28.5°$ and $\Delta i = 47.1°$

For the second case study, we modify the optimal control problem (28) by constraining the midpoint of the trajectory to a lower altitude band of 50–60 km. This condition allows the spacecraft to exploit higher atmospheric density, thereby increasing aerodynamic control authority and enabling larger inclination changes. We then evaluate two representative Low-Earth-Orbit (LEO) transfer missions: (i) a transfer from $i = 70°$ to sun-synchronous orbit (SSO) at $i = 98.7°$, requiring $\Delta i = 28.5°$, and (ii) a transfer from the ISS orbit ($i = 51.6°$) to SSO at 98.7°, requiring an inclination change of $\Delta i = 47.1°$.

3. Simulation Parameters

For this study, we iteratively varied the entry and exit altitudes, spacecraft mass, and aeroshell arm lengths, repeating the optimization until solver convergence was achieved. We also conducted a set of constrained optimization runs in which the arm deployment angles were restricted to remain near the maximum L/D configuration, with the angle of attack close to 9° and the bank angle near 90°. This choice reflects observations from [1], which reported that efficient skip trajectories for a given inclination change are dominated by maximizing lift-to-drag ratio at high bank angles. The simulation parameters used in this investigation are summarized in Table 2.

Table 2 Simulation Parameters and Constants

Parameter	Value	Parameter	Value
Earth radius, R_e	6.378137×10^6 m	Mass, m	1250 kg
Gravitational parameter, μ	3.986×10^{14} m^3/s^2	Arm length, L	4.52 m
Angular velocity, $\omega_\oplus$	7.292×10^{-5} rad/s	Nose radius, r_n	0.5 m
Sea-level density, ρ_0	1.225 kg/m^3	Angle of attack, α	−10° to 10°
Sea-level gravity, g_0	9.798 m/s^2	Bank angle, σ	−90° to 90°
Scale height, H	8.5×10^3 m	Sideslip angle, β	0°
Entry altitude, h_0	130 km	Max pressure coeff., $C_{p,\max}$	2

IV. Results & Discussion

When initially solving the optimization problem, the resulting trajectories were frequently trapped in suboptimal solutions. These solutions did not reproduce the ΔV efficiencies reported in [1] and, in some cases, even performed worse than a purely propulsive plane-change maneuver. In these cases, the optimizer relied heavily on side force rather than maximizing L/D, which proved ineffective for producing large inclination changes. To steer the solver toward physically realistic skip dynamics, we imposed stricter bounds on the arm angles and angle of attack to maintain geometries near the maximum L/D configuration (approaching the flat-plate limit, with side arms at 70° and top/bottom arms at 18°), while constraining the bank angle near 90°. Under these physically motivated constraints, the optimized morphing aeroshell demonstrated substantial reductions in total ΔV: approximately 24% for a 5° inclination change, 36% for a 10° change, 37% for a 15° change, and 38% for an 18° change. Beyond 18°, the ΔV required for re-circularization increases sharply. Figure 2 plots the comparison curve of the required ΔV for pure plane change maneuver and the skip-entry maneuver for case study-1. These results indicate that a modular shape-morphing aeroshell can enable practical and increasingly favorable fuel savings for larger skip-entry plane changes.

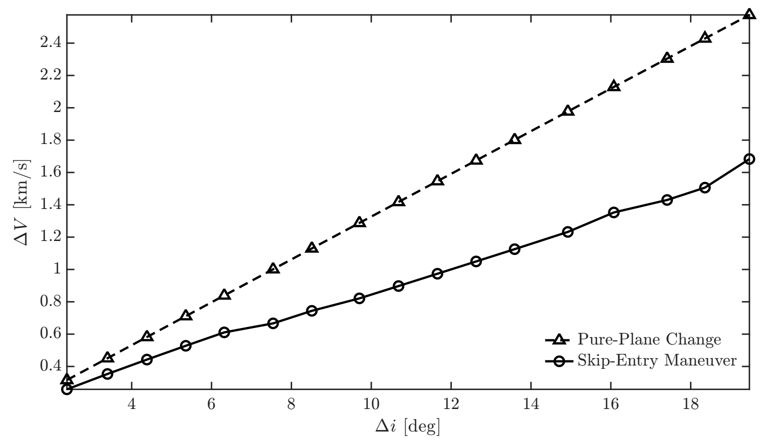

Fig. 2 ΔV vs. Δi for a pure propulsion-based plane change maneuver vs. a skip entry maneuver conducted using a modular shape morphing aeroshell.

Furthermore, we observed that tightening the bounds on the arm control angles, specifically constraining the top and bottom arms below 18° to maximize the vehicle's L/D ratio further reduced the ΔV required for a skip trajectory at a given inclination change. This trend is consistent with the efficiency gains reported in [1]. While these results are promising from a maneuverability and fuel-efficiency standpoint, they introduce practical limitations. In particular, extreme L/D configurations impose tighter volumetric constraints on the internal payload space, reducing the modularity of the aeroshell, and can induce prohibitively high aerothermal loads. Thus, there exists a clear trade-off between maximizing ΔV savings and maintaining a modular, thermally viable aeroshell capable of accommodating spacecraft with realistic dimensional constraints. This balance motivates further design and mission-level trade studies.

The skip-entry trajectories from Case Study 1 (Sec. III.F.1) are shown in Figure 3 for inclination changes of 5°, 10°, 15°, and 18°. As the inclination change increases, the spacecraft dips deeper into the atmosphere for higher aerodynamic control. During atmospheric reentry, convective heating is the dominant thermal load. To estimate this effect, we evaluated the stagnation-point heating rate using the Sutton–Graves correlation in (29) for skip maneuvers performing inclination changes of 5°, 10°, 15°, and 18°. Figure 4 shows the resulting heating-rate profiles over time for each case. As expected, larger inclination changes produce higher peak convective heating and steeper heating curves, due to shorter skip durations and deeper atmospheric penetration.

Table 3 summarizes key trajectory metrics, including maximum dynamic pressure, peak g-loads, total integrated heat load, and skip duration. For larger inclination changes, the spacecraft dips to lower altitudes to exploit increased aerodynamic control, resulting in higher dynamic pressure and g-loading. Peak heating rates rise with larger inclination changes, as they depend directly on both velocity and atmospheric density, which is greater at lower altitudes. Total integrated heat loads remain in the range of approximately 20–30 $\frac{KJ}{cm^2}$, primarily governed by the duration of the skip maneuver; larger inclination changes correspond to shorter maneuver times due to lower flight path angles at orbital reentry. Overall, the trajectories exhibit favorable characteristics manageable heating rates, maximum dynamic pressures, and peak g-loads comparable to past atmospheric reentry missions, indicating that the aeroshell and thermal

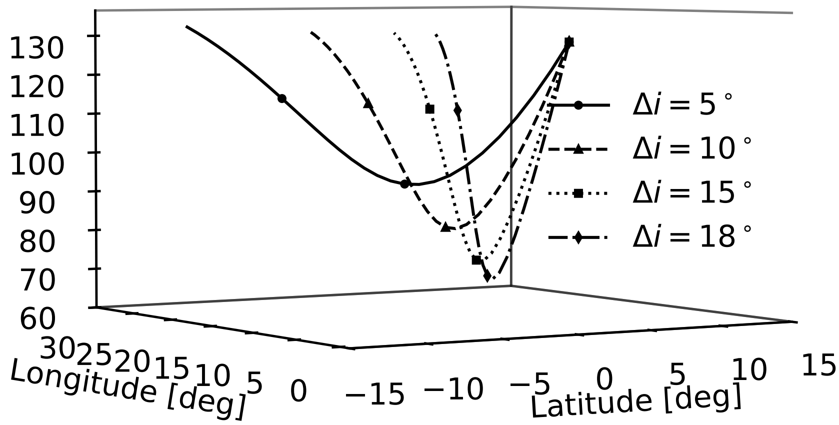

Fig. 3 Computed skip-entry trajectories for various Δi.

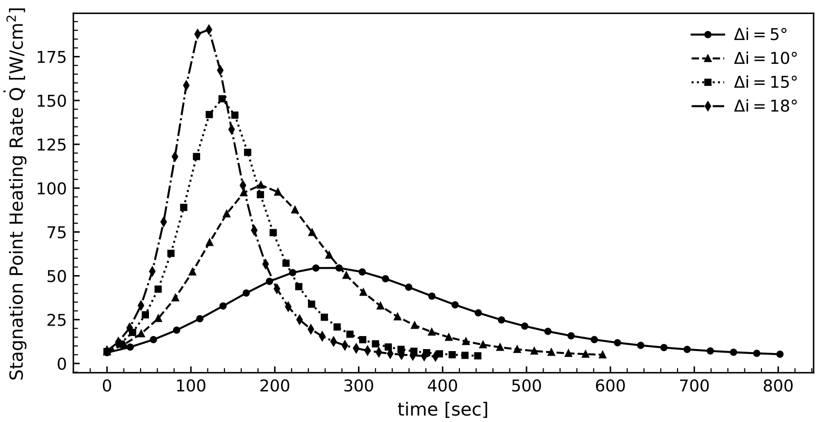

Fig. 4 Stagnation point convective heating rates for skip trajectories at various Δi.

protection system can be designed to safely shield the spacecraft during these maneuvers.

Table 3 Max dynamic pressure, max gloading, peak convective heating rates, total integrated heat loads, and skip duration for varying inclination change from case study 1 and case study 2

Δi (deg)	Max-Q (KPa)	$n_{\max}$ (g)	$\dot{Q}_{\max}$ (W/cm^2)	Tot. Integ. Heat Load (kJ/cm^2)	Skip Duration (s)
5	0.685	0.157	54.76	20.77	802
10	2.292	0.524	101.76	22.31	590.7
15	5.291	1.210	150.97	20.87	441.9
18	7.143	1.633	176.30	21.28	409.21
28.5	15.771	2.737	236.57	31.30	380.77
47.1	33.306	5.751	335.51	33.30	304.56

For Case Study 2 (Sec. III.F.2), which considers inclination change from the ISS orbit $i = 51.6^\circ$ to SSO 98.7°, of $\Delta i = 47.1^\circ$, the skip-entry maneuver requires 40% less ΔV (3.54 km/s), compared to 6.08 km/s using pure-plane change. For the orbital inclination change maneuver from $i = 70^\circ$ LEO to $i = 98.4^\circ$ SSO orbit, a $\Delta i = 28.4^\circ$, a pure-plane change maneuver at 500 km altitude would require $\Delta V_i = 2V\sin(\frac{\Delta i}{2}) = 3.73\text{km/s}$. In comparison, our proposed skip entry consumes only a total ΔV of 2.236 km/s, making it 40% more efficient. Table 3 summarizes the corresponding, maximum aerodynamic pressure, maximum g loading, convective heating rate, integrated heat rate, and skip duration.

Since the spacecraft is constrained at a lower altitude to enable higher aerodynamic authority, the maximum aerodynamic forces increase significantly for both the $\Delta i = 47.1^\circ$ and $\Delta i = 28.4^\circ$ cases. Similarly, the peak heating rate is also significantly higher, with shorter skip durations implying a steeper convective heating rate curve. Large inclination changes can be achieved with skip-entry maneuvers at a practical ΔV savings of around 40%, but this comes with trade-offs, including increased structural mass to withstand higher dynamic pressures and g-loads, as well as thicker thermal protection system (TPS) requirements, which must be further studied and optimized (Sec. V).

V. Conclusion

In this study, we demonstrated that a modular, shape-morphing aeroshell can enable practical ΔV savings for skip-entry orbital plane-change maneuvers. Using aerodynamic coefficients derived from modified Newtonian theory and a nonlinear optimal control formulation, we evaluated skip trajectories for varying inclination changes under realistic geometric and attitude constraints. When physically motivated bounds were imposed on the arm deflection angles, angle of attack, and bank angle to maintain high–lift-to-drag configurations, the optimized trajectories achieved approximately 24% ΔV savings for a 5° inclination change, 36% for 10°, 37% for 15°, and 38% for 18°, relative to a purely propulsive plane-change maneuver. These results indicate that the proposed variable-geometry aeroshell provides a feasible mechanism for leveraging atmospheric forces to reduce propulsive requirements during orbital reorientation. Although these findings establish initial feasibility, they do not represent the globally optimal aeroshell design. Improvements in lift-to-drag performance may be attainable by increasing the number of control arms, adjusting arm lengths, or modifying the effective nose radius. Each of these modifications, however, introduces competing aerothermal, structural, and volumetric trade-offs. For future work, a parametric, multi-objective design optimization can systematically balance aerodynamic performance, thermal protection requirements, structural feasibility, and spacecraft accommodation while minimizing total ΔV based on the mission use case and profile.

References

[1] Bettinger, R., Black, J., and Agte, J., "Design of Experiment Approach to Atmospheric Skip Entry Maneuver Optimization," *Journal of Spacecraft and Rockets*, Vol. 52, 2015, pp. 1–14. https://doi.org/10.2514/1.A33032.

[2] Bettinger, R., "Spacecraft Demand Tasking and Skip Entry Responsive Maneuvers," 2011, p. 165.

[3] Tauber, M. E., "Maximum Lift/Drag Ratio of Flat Plates with Bluntness and Skin Friction at Hypersonic Speeds," Technical Memorandum NASA TM-88338, NASA Ames Research Center, 1986. URL https://ntrs.nasa.gov/api/citations/19870002265/downloads/19870002265.pdf, accessed October 27, 2025.

[4] Hughes, S., Cheatwood, F., Dillman, R., Calomino, A., Wright, H., and DelCorso, J., "Hypersonic Inflatable Aerodynamic Decelerator (HIAD)Technology Development Overview," 2011. https://doi.org/10.2514/6.2011-2524.

[5] Slagle, A. C., "Morphing Hypersonic Inflatable Aerodynamic Decelerator (HIAD) Mechanisms and Controls," Ph.D. thesis, Virginia Polytechnic Institute and State University, June 2018. URL http://hdl.handle.net/10919/96194, ph.D. Dissertation.

[6] DiNonno, J., and Cheatwood, F., "Low-Earth Orbit Flight Test of an Inflatable Decelerator (LOFTID) Mission Overview and Science Return," 2024. https://doi.org/10.2514/6.2024-1309.

[7] Dutta, S., Karlgaard, C., Korzun, A., Green, J., Tynis, J., Williams, J., Yount, B., Cassell, A., and Wercinski, P., "Adaptable Deployable Entry and Placement Technology Sounding Rocket One Modeling and Reconstruction," *Journal of Spacecraft and Rockets*, Vol. 59, 2021, pp. 1–24. https://doi.org/10.2514/1.a35090.

[8] Dimino, I., Vendittozzi, C., Reis Silva, W., Ameduri, S., and Concilio, A., "A Morphing Deployable Mechanism for Re-Entry Capsule Aeroshell," *Applied Sciences*, Vol. 13, No. 5, 2023. https://doi.org/10.3390/app13052783, URL https://www.mdpi.com/2076-3417/13/5/2783.

[9] Fedele, A., "A Deployable Aerobraking System for Atmospheric Re-entry," Ph.D. thesis, 04 2020. https://doi.org/10.13140/RG.2.2.34074.36801.

[10] Regan, F. J., and Anandakrishnan, S. M., "Dynamics of atmospheric re-entry," *NASA STI/Recon Technical Report A*, Vol. 93, 1993, p. 50500.

[11] Young, F. D., "A General Stagnation-Point Convective-Heating Equation for Arbitrary Gas Mixtures," Tech. Rep. NASA R-376, NASA Langley Research Center, Hampton, VA, Nov. 1971. URL https://ntrs.nasa.gov/citations/19720003329, nASA Technical Report.

[12] Hicks, K., *Introduction to Astrodynamic Reentry*, CreateSpace Independent Publishing Platform, 2014. URL https://books.google.com/books?id=Wm_crQEACAAJ.

[13] Justus, C., Duvall, A., and Johnson, D., "Earth global reference atmospheric model (GRAM-99) and trace constituents," *Advances in Space Research*, Vol. 34, 2004, pp. 1731–1735. https://doi.org/10.1016/j.asr.2003.04.057.

[14] Vallado, D. A., *Fundamentals of Astrodynamics and Applications*, 5th ed., Microcosm Press, Portland, OR, 2022.

[15] Andersson, J. A. E., Gillis, J., Horn, G., Rawlings, J. B., and Diehl, M., "CasADi – A software framework for nonlinear optimization and optimal control," *Mathematical Programming Computation*, 2018.

[16] Wächter, A., and Biegler, L. T., "On the Implementation of a Primal-Dual Interior Point Filter Line Search Algorithm for Large-Scale Nonlinear Programming," *Mathematical Programming*, Vol. 106, No. 1, 2006, pp. 25–57.

[17] Tauber, M. E., and Sutton, K., "Stagnation-Point Radiative Heating Relations for Earth and Mars Entries," *Journal of Spacecraft and Rockets*, Vol. 28, No. 1, 1991, pp. 40–42. https://doi.org/10.2514/3.26206, URL https://doi.org/10.2514/3.26206.